JOURNAL OF THE KOREAN ASTRONOMICAL SOCIETY
38: 197 ~ 201, 2005

EVOLUTION OF SELF-GRAVITATING GAS DISKS UNDER THE INFLUENCE OF A ROTATING BAR POTENTIAL

CHI YUAN[1,2] AND DAVID C. C. YEN[1,3]
[1]Institute of Astronomy & Astrophysics, Academia Sinica, Taipei, Taiwan
E-mail: yuan@asiaa.sinica.edu.tw
[2]Physics Department, National Taiwan University, Taipei, Taiwan
[3]Mathematics Department, Fu Jen Catholic University, Hsinchung, Taipei, Taiwan
(Received February 1, 2005; Accepted March 15, 2005)

ABSTRACT

It is well known that a rotating bar potential can transport angular momentum to the disk and hence cause the evolution of the disk. Such a process is particularly important in disk galaxies since it can result in fuelling AGNs and starburst ring activities. In this paper, we will present the numerical simulations to show how this mechanism works. The problem, however, is quite complicated. We classify our simulations according to the type of Lindbald resonances and try to single out the individual roles they play in the disk evolution. Among many interesting results, we emphasize the identification of the origin of the starburst rings and the dense circumnuclear molecular disks to the instability of the disk. Unlike most of the other simulations, the self-gravitation of the disk is emphasized in this study.

Key words : Lindblad resonance — bar-driven density waves — Toomre instability

I. INTRODUCTION

This article deals with three extra-ordinary phenomena observed in the central region of the nearby galaxies, namely, the starburst rings, the dense circumnuclear molecular disks and the apparent gas "hole" towards the galactic center. We will show all these three phenomena are related to a fast rotating bar potential in the center. Starburst rings are best exempted by the pictures displayed by the HST website. Shown in Figure 1 are starburst rings in NGC1512 and NGC4314, and the diamond-shaped double rings in NGC6782. To be emphasized is that all these "rings" in NGC1512 and NGC4314 are tightly wound spirals.

The dense circumnuclear molecular disks (CNMD) are gaseous disks of high density and moderate high temperature (100K) with a typical radius a few hundred parsecs surrounding the center. They are seen in many galaxies, including the Milky Way (Jackson et al 1996), NGC1068 (Bruhwieler et al, 2001), and M51 (See S. Matsushita's article in this issue). The gas hole toward the center has been known ever since the early observations of HI in M31, M81 and the Milky Way. Later observations reveal that this hole exists also for molecular gas and it is common in many nearby galaxies.

In this paper, we will show that a fast rotation bar potential can generate these three features altogether, through a resonance excitation mechanism. The starburst rings can be identified with spiral density waves associated with the outer Lindblad resonance (OLR)

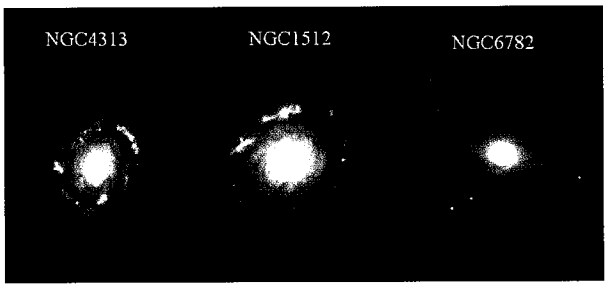

Fig. 1.— Starburst rings: The left are starburst rings about 1 kpc from the center. The right shows a double rings. Pictures taken from STSI website, credits for NGC6782: NASA and the Hubble Heritage team; NGC1512: NASA, ESA and D. Maos; NGC4314: G. F. Benedict, A. Howell, I. Jorgensen, D. Chapell, J. Kenney, and B. J. Smith, and NASA

and the dense CNMD, with the inner Lindblad resonance (ILR). The angular momentum transport from the bar to the disk or vice versa through the resonance excitation mechanism, which is manifested in terms of spiral waves, will gradually open a wide gap between the two resonances to form the "hole" between them. This is the origin of these observed gas "holes" toward the galactic center. Furthermore, we will show the starburst rings and CNMD phenomena are closely related to the disk stability. In the location of the OLR, the high density in the spirals will lead to gravitational instability in Toomre's sense, which results in massive star formation activity, the starburst rings. On the other hand, in the location of the ILR, high inertia force in the galactic center is capable of preventing the gas disks from gravitational collapse, despite of the ex-

Proceedings of *the 6th East Asian Meeting of Astronomy*, held at Seoul National University, Korea, from October 18-22, 2004.

tremely high surface density of the gas. This explains the origin of the dense CNMD.

We will use numerical simulations to demonstrate the above scenario in this paper. In what follows, we first specify the bar potential, the rotation curves, and initial distribution of the gas density for the simulations(section 2). The numerical methods, the Antares code, are described in section 3. Then, we present results of a single OLR and the combination of the OLR and the ILR (sections 4) to stress the different roles played by the two resonances. In section 5, we discuss two issues related to the calculations: the Toomre instability and the gap opening mechanism. Other remarks on the calculations are also to be found there.

II. THE DISK MODEL AND THE BAR POTENTIAL

For the simulations discussed in this paper, we adopt two model rotation curves. For the first one, we choose the one used by Elmegreen & Elmegreen (1990), which can be expressed as

$$V = V_0 \frac{r}{r^B + r^{1-A}}, \tag{1}$$

where r is a dimensionless radius, normalized by 1 kpc, $V_0 = 300\ km/s$, and $B = 0$ and $A = -0.1$. This rotation curve rises slowly from the center and reaches a nearly constant value about 220 km/s outside. Since $V \sim r$ near the galactic center, hence the epicyclic frequency $\kappa \simeq 2\Omega$, the $\Omega - \kappa/2$ curve drops to zero at the center and has a maximum in the central region. If Ω_p is greater than the maximum of $\Omega - \kappa/2$, it only intersects with the $\Omega + \kappa/2$ curve, hence only one resonance, the OLR, also shown in the right panel of Figure 2. This will be the first case of our simulations. The rotation curve is depicted in the left panel of Figure 2.

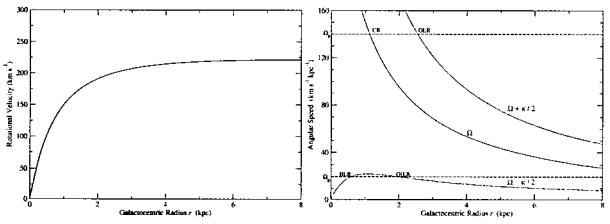

Fig. 2.— Elmegreen rotation curve (slowly rising). The left panel is the rotation speed in km/s vs. radius in kpc. In the right panel, the middle curve is angular velocity Ω, and the top curve and bottom curve are respectively the $\Omega + \kappa/2$ and $\Omega - \kappa/2$, all in km/s-kpc. The two horizontal lines represent speeds of the bar rotation. The radii of the intersections with the $\Omega + \kappa/2$ curve and the $\Omega - \kappa/2$ curve are the locations of Lindblad resonances. We only consider the top horizontal line in this paper.

The second rotation curve is the nearly flat one, which is

$$V = V_0 (\frac{r}{r+\epsilon})^{1/2}, \tag{2}$$

with $\epsilon = 0.01$. It rises rapidly from the center, representing high concentration of mass in the center. In this case, the $\Omega - \kappa/2$ curve does not have a local maximum. The pattern speed of the bar, Ω_p, would intersect with $\Omega \pm \kappa/2$ curves, resulting two Lindblad resonances, the ILR and OLR, as shown in Figure 3.

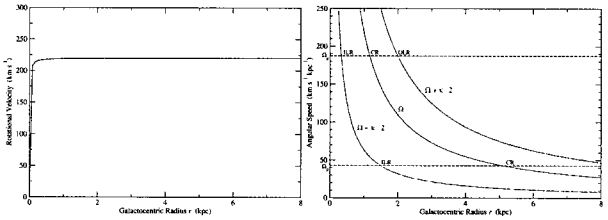

Fig. 3.— Nearly flat rotation curve (fast rising). The left panel is the rotation speed in km/s vs. radius in kpc. In the right panel, the middle curve is angular velocity Ω, and the top curve and bottom curve are respectively the $\Omega + \kappa/2$ and $\Omega - \kappa/2$, all in km/s/kpc. The two horizontal lines represent speeds of bar rotation. The intersection of ILR and OLR by the upper line are to be considered here.

The bar potential is taken to be

$$\mathcal{V} = \Psi \cos\theta, \tag{3}$$

with

$$\Psi = \Psi_0 \frac{r^2}{(a^2 + r^2)^2}, \tag{4}$$

where a is at the potential minimum. This potential has the property that it goes to zero as r^2 and approaches r^{-2} for large r. Thus, the bar force at $r = 0$ is zero, while it behaves as r^{-3} (not r^{-2}) when r is large. In other words, the axisymmetric component of the bar potential has been removed.

The initial gas density is set to be constant for the cases of non-self-gravitating disks, in which we simply take $\sigma/\sigma_0 = 1$, where σ is the surface density. For the self-gravitating disks, we use

$$\sigma = \sigma_0 e^{-(\frac{r}{r_0})^2}, \tag{5}$$

where σ_0 is the initial surface density at the center and usually we take a value of 50 $M_\odot - pc^{-2}$. The value of r_0 is specified by $\sigma = (1/5)\sigma_0$ at $r = 3$ kpc.

III. THE ANTARES CODE

The Antares Code has two main systems: the relaxation and the high-order Godunov. Both are available in Cartesian and polar coordinates. At present, the codes are written for 2-dimensional Euler equations coupled with the Poisson equation for an infinitesimally thin disk and the gas is assumed either isothermal or polytropic. The relaxation codes were written earlier and are slightly more dissipative than the high-order Godunov codes, but less time consuming. The high-order Godunov codes are based on the idea to calculate

the flux on the interfaces, using the exact Riemann solution, while the relaxation codes use an approximate Riemann solution (Jin & Xin 1995) . Both codes adopt the van Leer type limiters and dependent variables are piecewise linear from cell to cell, so of the 2nd order accuracy. For both codes, discretization only applies to the space variables, so they are semi-discretization codes. We advance discretized system of equations in time by 2nd order Runge-Kutta method (RK2). The contributions of the source terms enter through RK2.

Cartesian coordinates avoid the inner boundary conditions for the problem, which is most convenient for the galaxy problems. They are adopted in the present computation. At the outer boundary, we impose radiation boundary conditions. We perform charateristics decomposition in each boundary cell and allow waves to go out and stop incoming waves. Thus, it guarantees no reflection on the boundary.

The Poisson equation for disk problems is intrinsically 3-dimensional. We are thus not to solve the complete potential function problem, rather simply to calculate the force in the plane by integration. The force in each cell can be written as a double summation of the product of surface density and a convolution kernel. Using fast Fourier transform, we can reduce the entire computation for force from $N^2 \times N^2$ to $N^2(\ln N)^2$. Furthermore, our Poisson solver does not require the periodic boundary condition. We are making it of second-order accuracy and parallelized.

All our codes used in the calculations must pass three tests: (1) Exact smooth solutions remain 2nd order accuracy as long as our simulation lasts. (2) Basic states remain unchanged for as long as our simulation runs (the balance law problem) (3) Non-reflection boundary condition holds. Although codes are still two-dimensional and without many advanced features such as AMR, we think they are among the most accurate and reliable codes available today.

IV. NUMERICAL RESULTS

In this section, we present our numerical simulations according to the resonance, first the single resonance and then the combination of them. At the same time, we point out the relevant observations that they may be responsible for. When we refer to the theory in the following context, we mean the non-linear asymptotic theory of resonantly excited spiral density waves in galaxies developed by us (Yuan & Cheng 1991; Yuan & Kuo 1997).

The OLR and Starburst Rings We use the Elmegreen rotation curve and a fast rotating bar such that only OLR exists (See Figure 2). With pattern speed $\Omega_p = 140\ km/s$, the OLR occurs at $r = 2\ kpc$. The result is a pair of tightly wound spirals being generated at the OLR with no central features present, exactly as the asymptotic theory predicts. Since at OLR, the bar transports angular momentum to the disk. The disk material near the resonance gains angular momentum and moves out. It eventually clear a gap behind it. After 8 turns of the bar, the ring-like spirals are in close resemblance to the starburst ring seen in NGC4313. Inside the spiral-ring is a wide region void of gas. However, when self-gravity of the disk is included, the spirals become unstable and develop into chaos. This is because the rapid increase of surface density, σ, in the narrow spiral-ring region forces the Toomre's $Q = a\kappa/\pi G\sigma$ there to go under 1 and thus turn that region into instability. These are shown in Figure 4. The point to be stressed is that there is no central features in this case, since there is no ILR.

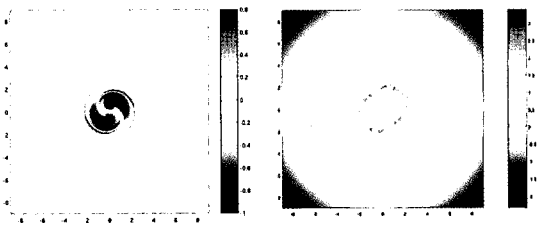

Fig. 4.— Surface density for single OLR. Spiral waves are excited at 2 kpc by a fast bar potential, lying in the horizontal direction. The high density spiral regions would lead to starbust activities as shown in the right panel is when the self-gravity of the disk is introduced.

The OLR-ILR Combination If the ILR exists and is close to the center, an oval disk with spirals imbedded in it is formed near the center. The central oval disk is gravitationally stable even with extremely high surface density, upto $10^3\ M_\odot/pc^2$. This is because the high values of epicyclic frequency κ near the center cancel out the high surface density so Toomre's Q, defined as $Q = \kappa a/(\pi G\sigma_0)$, remains greater than 1. So it survives in the self-gravitation case. The result explains the origin of the CNMD observed in many nearby galaxies. Because the spiral waves propagate in the opposite directions, the OLR and ILR do not interfere with each other. However, they join force to clear the gap between them. As we just explained, the waves at OLR move the gas there to form the spiral-ring, while the waves at the ILR moves the gas in the central disk to form the dense CNMC. The spiral-ring structure eventually becomes unstable due to the sharp rise of their surface density while the epicyclic frequency remains low there. The instability leads to starburst activities in the spiral-ring structure. This is the case for NGC1068 (Bruhweiler et al 2001) and for the Milky Way with the 3-kpc arm outside (Yuan & Cheng 1991) and a dense CNMD at the center (Jackson et al 1996). Nevertheless, when the OLR and ILR are not separated so far away, they may weakly interfere and give rise to the diamond-shape feature between the two resonances.

This will be relevant to the observation of the double rings in NGC6782. Given the limited space here, the result is not shown here.

Shown in Figure 5 are the results of simulations for the combination of both OLR and ILR, with and without disk self-gravitation. We use a rotation curve slightly different from the nearly flat rotation in figure 3, in order to have OLR situated at 3 kpc and ILR at 0.5 kpc, more or less to simulate the Milky Way. All three phenomena are present: Starburst ring, the dense CNMD and the "hole" of gas between them.

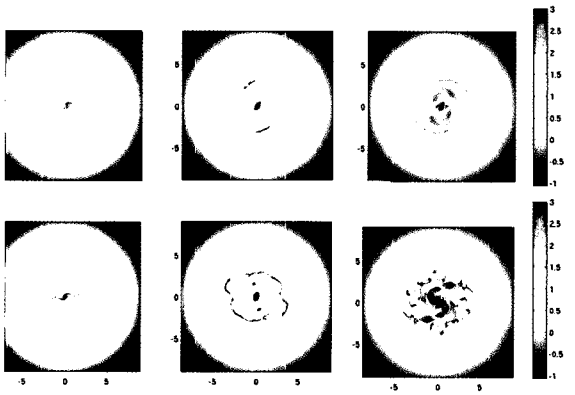

Fig. 5.— OLR-OILR combination. Spiral patterns excited by a bar at OLR (at 3 kpc) and at OILR (at 0.5 kpc) are shown here at 1, 4 and 8 turns of the bar. The top panels are for non-self-gravitation while the bottom panels for self-gravitation. the inner oval disk can be identified as the observed dense CNMD, which is stable even in the self-gravitational case. The outer spiral-ring structure develops into starburst rings. Also notice the gas gap between OLR and ILR.

The instability at OLR can be identified to be of Toomre's kind. In figure 6, we plot the Toomre's Q value at the onset of instability, which occurs at the 3rd turn of the bar. We can see it coincides with Q when it dips under 1 at $r = 3\ kpc$. On other hand, in the center where the CNMD is located, the surface can go as high as $10^3\ M_\odot/pc^2$. The disk remains mainly stable, except along the spirals where shock waves occur.

V. CONCLUDING REMARKS

We have shown that the starburst ring, the dense CNMD, and a gas-void region between them in the central region of a disk galaxy can be produced by a fast rotating bar potential. The starburst ring can be identified as a phenomenon associated with the OLR, while the dense CNMD, the ILR. The gas-void region, or the "hole", between them is a result of gap clear by the spiral density waves excited at the two resonance. Not every disk galaxy is capable of doing this. In order to have both OLR and ILR in the galactic central regions, we need a rapidly rising rotation curve, such as the one in the Milky Way. Rapidly rising rotation

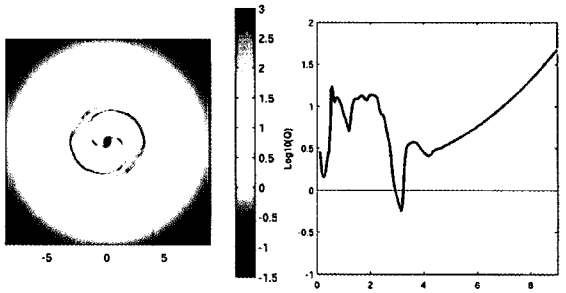

Fig. 6.— Onset of instability at time equal to 3 turns of the bar. Left is the surface density and right is the Q-value average on a circular ring. The instability starts to grow once Q dips below 1, or 0 on logarithmic scale

curve implies high concentration matter at the center. High concentration of matter with rapid rotation tends to develop Jacobi type of ellipsoids, which would act as a fast nuclear bar and in turn to produce the three observed phenomena we discuss in this paper.

If the rotation does not rise rapidly enough, such as the Elmegreen's rotation curve in figure 2, we may still have the starburst ring phenomenon and the partial gap-clearing inside the spiral-ring structure, provided there is a fast rotating bar. But in this case, there will be no dense CNMD as shown in the last section.

Toomre's instability criterion works extremely well here. The onset of instability sets in as soon as the Q-value dips below 1. The system then develops into chaos. Since Toomre's criterion is derived for the axisymmetric disturbance. One would wonder why it works so well, even when disturbance breaks into chaotic patterns. The reason may lie in the fact that the instability occurs at small length scale, which belongs to the left branch of the neutral stability curve of Toomre's (e.g., Lin and Lau 1975). That part is insensitive to the change of the circumferential Fourier wavenumber m.

ACKNOWLEDGEMENTS

The Antares code is developed in addition to the present authors by Drs. I-Liang Chern and Wei-Chen Wang and Mr. C.C. Yang. The work is supported in parts by a Key Project of Academia Sinica and National Science Council grant 93-2112-M-001-010.

REFERENCES

Bruhweiler, F. C., Miskey, C. L.; Smith, A. M., Landsman, W., & Malumuth, E., 2001 ApJ, 546, 866

Elmegreen, B. G., & Elmegreen, D. M., 1990, ApJ, 355,52

Jackson, J. M., Heyer, M. H., Paglione, T. A. D., & Bolatto, A, D., 1996, ApJ, 456, L91

Jin, S., & Xin, Z. P., 1995, Commun. Pure Appl. Math., 58, 235

Lin, C. C., & Lau, Y. Y., 1975, SJAM, 29, 352
Yuan, C., & Cheng, Y., 1991, ApJ, 376, 104
Yuan, C., & Kuo, C. L., 1997, ApJ, 486, 750
Yuan, C., & Chao-lin Kuo, 1998, ApJ, 497, 689